

Received July 3, 2016, accepted July 20, 2016, date of publication July 27, 2016, date of current version October 31, 2016.

Digital Object Identifier 10.1109/ACCESS.2016.2594187

# Electrical Anisotropic Response of Water Conducted Fractured Zone in the Mining Goaf

BENYU SU<sup>1,2</sup>, REZA MALEKIAN<sup>3</sup>, (Member, IEEE), JINGCUN YU<sup>1,2</sup>,  
XIHUI FENG<sup>4</sup>, AND ZHIXIN LIU<sup>2,5</sup>

<sup>1</sup>School of Resources and Geosciences, China University of Mining and Technology, Xuzhou 221116, China

<sup>2</sup>State Key Laboratory for Geomechanics and Deep Underground Engineering, China University of Mining and Technology, Xuzhou 221116, China

<sup>3</sup>Department of Electrical, Electronic and Computer Engineering, University of Pretoria, Pretoria 0002, South Africa

<sup>4</sup>Key Laboratory of Coal Resource Exploration and Comprehensive Utilization, Ministry of Land and Resources, Xian 710054, China

<sup>5</sup>School of Resource and Earth Science, China University of Mining and Technology, Xuzhou 221116, China

Corresponding author: Z. Liu (liuzhixincumt@163.com)

This work was supported in part by the Jiangsu Province National Natural Science Foundation under Grant BK20130180, in part by the Research Funds for the Central Universities within the China University of Mining and Technology under Grant 2014QNA88, and in part by the China Postdoctoral Science Foundation under Grant 2015M570491.

**ABSTRACT** Based on the Maxwell equation, the occurrences of fractured zones are studied through the galvanic method. The electrical and magnetic fields are first derived in the spatial domain. To simplify the calculations, the computational formulas of the electrical fields in the spatial domain are transformed into the wavenumber domain by the Fourier transform. The basic solution of the electromagnetic field can thus be easily solved in the wavenumber domain. According to the boundary conditions, a recursive relationship between the different layers is established. The electromagnetic fields are obtained through the recursive relationships with the bottom-last layer. Finally, the apparent resistivity is calculated using the surface electric field. A typical goaf model is used for the numerical simulation. Based on the modeling results, the effectiveness of this method is determined. The modeling results indicate that the galvanic method is very effective for detecting the electrical anisotropic characters.

**INDEX TERMS** Electrical anisotropic characteristics, mining goaf, electromagnetic fields, computation of apparent resistivity, numerical simulation.

## I. INTRODUCTION

As is common knowledge, water inrush is the first issue to be resolved during coal mining production. There are several reasons which cause water inrush, of which the goaf is the dominant one. The geological structure of the goaf is composed of three zones: bending zone, fracture zone and caving zone. The main reason for the water inrush by the goaf is that water at the ground surface of the bending zone accumulates at the surface of the bending zone. If the water rushes into the goaf via fractures of the fracture zone, it will result in a mining disaster. It is thus very important to detect the geological occurrence of the fractures in the fractured zone for prevention and governance of mining water flooding caused by the goaf.

Common geophysical methods used for exploring the goaf are: seismic method, resistivity method and geological radar method. However, for the seismic and geological radar method, the basis of geology is thought to be layered

structure and the resistivity method usually does not consider anisotropy. These methods thus cannot detect the fractured information such as dips and strikes, which are very important for governance of the goaf. The geological structure of the fractured zone is anisotropic; thus incorrect geological conclusions are often deduced from the data measured using the traditional electrical resistivity method. In this paper, based on the Maxwell equation and considering the electrical anisotropic characters of the goaf, a formula of the apparent resistivity is presented.

Systematic studies have been done in relation to the formation of electrical characteristics. According to the results of numerical simulation and actual applications [4], the conductivity of formation will increase if the fractures exist in the formation of high resistivity. Asten [5] and Matias and Habberjam [6] analyzed the effect of fractures and structures on the electrical anisotropy. In addition, Chlamtac and Abramovici [7] and

Anderson et al. [8] studied the relationship between apparent resistivity and real resistivity in the layered formation. Furthermore, Li et al. [9] analyzed the relation between electromagnetic response and formation anisotropy. Yin and Weidelt [11] and Shen et al. [12] have suggested the formula to calculate apparent resistivity of anisotropic formation. In addition, Han et al. [13] and Jing et al. [14] have studied the stability of anisotropic and non-homogeneous slopes using limit analysis. According to the studies however, anisotropic characters of the fractured zone in the form of apparent resistivity can be used to indicate the geologic occurrence. Therefore, the rules of formation fracture in the fractured zone will be significant for water hazard prevention of the mine shaft.

The purpose of the paper is to study the fracture occurrence of the fractured zone, such as the strike direction and dip angle of the fracture, as shown in Figure 1. Based on the above studies, the rules of electrical anisotropic response are observed in order to analyze the characteristics of the fracture distributions.

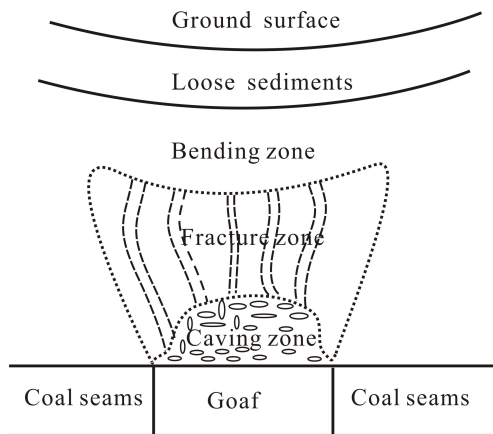


FIGURE 1. Geological model of the goaf (as taken from Su et al. [15]).

## II. METHODOLOGY

### A. EQUATION OF ELECTROMAGNETIC FIELD IN THE ANISOTROPIC MEDIA

Propagation of the electromagnetic field and the distribution of the current density in the earth meet the Maxwell equation [16]:

$$\nabla \times E = 0, \quad \nabla \cdot J = 0 \quad (1)$$

$$\nabla \times H = J, \quad \nabla \cdot B = 0, \quad H\mu = B \quad (2)$$

$$J = \hat{\sigma}E + J_e, \quad \hat{\sigma} = \hat{\rho}^{-1}, \quad \hat{\rho} = \begin{bmatrix} \rho_{xx} & \rho_{xy} & \rho_{xz} \\ \rho_{yx} & \rho_{yy} & \rho_{yz} \\ \rho_{zx} & \rho_{zy} & \rho_{zz} \end{bmatrix} \quad (3)$$

Where,  $\mu$  is magnetic permeability and  $\sigma$  are conductivity tensors, respectively.  $E$  and  $H$  are the electric field and magnetic field respectively.  $J$  is the total current density and  $J_e$  is the source current density.

The magnetic field  $H$  and current density  $J$  can be further described by the following formulas using a toroidal and a poloidal scalar [17].

$$H = \nabla \times (\hat{z}T_H) + \nabla \times \nabla \times (\hat{z}P_H) \quad (4)$$

$$J = \nabla \times (\hat{z}T_J) + \nabla \times \nabla \times (\hat{z}P_J) \quad (5)$$

Here,  $\hat{z}$  is the unit vector in  $z$  direction,  $T_J$  and  $P_H$  are the electrical toroidal scalar potential and the magnetic poloidal scalar potential respectively. Conversely,  $T_H$  and  $P_J$  are the magnetic toroidal scalar potential and the electrical poloidal scalar potential respectively. Obviously,  $T_J = 0$ ,  $P_J = 0$  in the air ( $z < 0$ ).

For the formula  $H = \nabla \times (\hat{z}T_H) + \nabla \times \nabla \times (\hat{z}P_H)$  in Equation 4:

$$\nabla \times (\hat{z}T_H) = \begin{bmatrix} i & j & k \\ \frac{\partial}{\partial x} & \frac{\partial}{\partial y} & \frac{\partial}{\partial z} \\ 0 & 0 & T_H \end{bmatrix} = i \frac{\partial T_H}{\partial y} - j \frac{\partial T_H}{\partial x} \quad (6)$$

In the same way the following can be obtained:

$$\nabla \times (\hat{z}P_H) = \begin{bmatrix} i & j & k \\ \frac{\partial}{\partial x} & \frac{\partial}{\partial y} & \frac{\partial}{\partial z} \\ 0 & 0 & P_H \end{bmatrix} = i \frac{\partial P_H}{\partial y} - j \frac{\partial P_H}{\partial x} \quad (7)$$

Next the curl of the formula is determined:

$$\nabla \times (\hat{z}P_H) = \begin{bmatrix} i & j & k \\ \frac{\partial}{\partial x} & \frac{\partial}{\partial y} & \frac{\partial}{\partial z} \\ 0 & 0 & P_H \end{bmatrix} = i \frac{\partial P_H}{\partial y} - j \frac{\partial P_H}{\partial x} \quad (8)$$

$$\begin{aligned} \nabla \times \nabla \times (\hat{z}P_H) &= \begin{bmatrix} i & j & k \\ \frac{\partial}{\partial x} & \frac{\partial}{\partial y} & \frac{\partial}{\partial z} \\ \frac{\partial P_H}{\partial y} & -\frac{\partial P_H}{\partial x} & 0 \end{bmatrix} \\ &= i \frac{\partial^2 P_H}{\partial x \partial y} - j \frac{\partial^2 P_H}{\partial x \partial z} - k \left( \frac{\partial^2 P_H}{\partial x^2} + \frac{\partial^2 P_H}{\partial y^2} \right) \end{aligned} \quad (9)$$

Combining Equation 8 and Equation 9, the magnetic field  $H$  can be obtained:

$$\begin{aligned} H &= \nabla \times (\hat{z}T_H) + \nabla \times \nabla \times (\hat{z}P_H) \\ &= i \left( \frac{\partial^2 P_H}{\partial x \partial z} + \frac{\partial T_H}{\partial y} \right) + j \left( \frac{\partial^2 P_H}{\partial y \partial z} + \frac{\partial T_H}{\partial x} \right) \\ &\quad - k \left( \frac{\partial^2 P_H}{\partial x^2} + \frac{\partial P_H}{\partial y^2} \right) \end{aligned} \quad (10)$$

The magnetic field  $H$  in the horizontal wavenumber domain can be obtained by the Fourier transform formula:

$$\tilde{F}(u, v) = \int_{-\infty}^{+\infty} \int_{-\infty}^{+\infty} F(x, y) e^{-i(k_x x + k_y y)} dx dy \quad (11)$$

Here,  $k_x$ ,  $k_y$  are wave number in x-direction and y-direction.

Hence Equation 10 can be transformed into:

$$\begin{aligned} \tilde{H}(u, v) &= \int_{-\infty}^{+\infty} \int_{+\infty}^{+\infty} (i(\frac{\partial^2 P_H}{\partial x \partial z} + \frac{\partial T_H}{\partial y}) + j(\frac{\partial^2 P_H}{\partial y \partial z} - \frac{\partial T_H}{\partial x}) \\ &\quad - k(\frac{\partial^2 P_H}{\partial x^2} + \frac{\partial^2 P_H}{\partial y^2})) e^{-i(ux+vy)} dx dy \\ &= (iu\tilde{P}'_H + iv\tilde{T}_H, jv\tilde{P}'_H - ju\tilde{T}_H, k^2\tilde{P}_H)^T \end{aligned} \quad (12)$$

As with the calculation of  $H$ , current density  $J$  in the space domain can also be obtained:

$$J = i(\frac{\partial^2 P_J}{\partial x \partial z} + \frac{\partial T_J}{\partial y}) + j(\frac{\partial^2 P_J}{\partial y \partial z} - \frac{\partial T_J}{\partial x}) - k(\frac{\partial^2 P_J}{\partial x^2} - \frac{\partial P_J}{\partial y^2}) \quad (13)$$

The current density  $J$  in the wavenumber domain can be obtained via the Fourier transform formula:

$$\tilde{J} = (iv\tilde{T}_J + iu\tilde{P}'_J, -iu\tilde{T}_J + iv\tilde{P}'_J, k^2\tilde{P}_J)^T \quad (14)$$

According to the Equation 2, the following formula can be obtained:

$$(\nabla \times H - J) = 0, \quad \hat{z}(\nabla \times H - J) = 0 \quad (15)$$

The curl of magnetic field  $H$  can be expressed as:

$$\begin{aligned} \nabla \times H &= [\frac{\partial}{\partial y}(\frac{\partial^2 P_H}{\partial x^2} + \frac{\partial^2 P_H}{\partial y^2}) - \frac{\partial}{\partial z}(-\frac{\partial T_H}{\partial x} + \frac{\partial^2 P_H}{\partial y \partial z}), \\ &\quad \times((\frac{\partial}{\partial z})(\frac{\partial T_H}{\partial y} + \frac{\partial^2 P_H}{\partial x \partial z}) - \frac{\partial}{\partial x}(\frac{\partial^2 P_H}{\partial x^2} + \frac{\partial^2 P_H}{\partial y^2})), \\ &\quad \times(\frac{\partial}{\partial x})(-\frac{\partial T_H}{\partial x} + \frac{\partial^2 P_H}{\partial y \partial z}) - \frac{\partial}{\partial y}(\frac{\partial T_H}{\partial y} + \frac{\partial^2 P_H}{\partial x \partial z})] \end{aligned} \quad (16)$$

Hence, the curl of the magnetic field in the x-direction can be obtained.

$$\begin{aligned} \hat{z} \cdot (\nabla \times H) &= \frac{\partial}{\partial x}[\frac{\partial^2 P_H}{\partial x \partial z} - \frac{\partial T_H}{\partial x}] - \frac{1}{\partial y}[\frac{\partial T_H}{\partial y} + \frac{\partial^2 P_H}{\partial y \partial z}] \\ &= -[\frac{\partial^2 T_H}{\partial x^2} + \frac{\partial^2 T_H}{\partial y^2}] \end{aligned} \quad (17)$$

According to Equation 13, the current density in the z-direction can be expressed using Equation 18:

$$\hat{z}(J) = -[\frac{\partial^2 P_J}{\partial x^2} + \frac{\partial^2 P_J}{\partial y^2}] \quad (18)$$

Based on Equation 15, 17 and 18, we can obtain the following conclusions:

$$\hat{z}(\nabla \times H) = \hat{z}(J), \quad T_H = P_J \quad (19)$$

The curl of the second item of Equation 15 can be described using Equation 20.

$$z \cdot [\nabla \times (\nabla \times H)] = z \cdot [\nabla \times (J)] \quad (20)$$

The left part of Equation 20, is deduced as shown below:

$$\begin{aligned} \hat{z} \cdot [\nabla \times (\nabla \times H)] &= \frac{\partial}{\partial x^2}[\frac{\partial^2 P_H}{\partial z^2} - (\frac{\partial^2 P_H}{\partial x^2} + \frac{\partial^2 P_H}{\partial y^2})] \\ &\quad + \frac{\partial}{\partial y^2}[\frac{\partial^2 P_H}{\partial z^2} - (\frac{\partial^2 P_H}{\partial y^2} + \frac{\partial^2 P_H}{\partial x^2})] \end{aligned} \quad (21)$$

The right part of Equation 20 is deduced, as shown in Equation 22.

$$\begin{aligned} \hat{z} \cdot [\nabla \times J] &= -\frac{\partial}{\partial y}(\frac{\partial T_J}{\partial y} + \frac{\partial^2 P_J}{\partial x \partial z}) + \frac{\partial}{\partial x}(-\frac{\partial T_J}{\partial x} + \frac{\partial^2 P_J}{\partial y \partial z}) \\ &= -(\frac{\partial^2 T_J}{\partial y^2} + \frac{\partial^2 T_J}{\partial x^2}) \end{aligned} \quad (22)$$

Based on Equation 21 and 22, the following can be obtained:

$$\begin{aligned} \frac{\partial}{\partial x^2}[\frac{\partial^2 P_H}{\partial z^2} - (\frac{\partial^2 P_H}{\partial x^2} + \frac{\partial^2 P_H}{\partial y^2})] + \frac{\partial}{\partial y^2}[\frac{\partial^2 P_H}{\partial z^2} \\ - (\frac{\partial^2 P_H}{\partial y^2} + \frac{\partial^2 P_H}{\partial x^2})] = -(\frac{\partial^2 T_J}{\partial y^2} + \frac{\partial^2 T_J}{\partial x^2}) \end{aligned} \quad (23)$$

The shorthand of Equation 23 can be described as:

$$T_J = -\nabla^2 P_J \quad (24)$$

The expression in the wavenumber domain of Equation 24 can be deduced via the Fourier transform.

$$\tilde{T}_J = k^2\tilde{P}_H - \tilde{P}''_H \quad (25)$$

According to ohm's law, there exists a relationship among the current density, electrical field and conductivity.

$$J = \hat{\sigma} E \quad (26)$$

Equation 26 can be rewritten as:

$$E = \hat{\rho} J \quad (27)$$

Here,

$$\hat{\rho} = \begin{bmatrix} \rho_{xx} & \rho_{xy} & \rho_{xz} \\ \rho_{yx} & \rho_{yy} & \rho_{yz} \\ \rho_{zx} & \rho_{zy} & \rho_{zz} \end{bmatrix}$$

Based on Equation 27, Equation 1 can be expressed as:

$$\nabla \times (\hat{\rho} J) = 0 \quad (28)$$

Furthermore, the curl of Equation 28 can be obtained, as follows:

$$\nabla \times \nabla \times (\hat{\rho} J) = 0 \quad (29)$$

For the  $(\hat{\rho} J)$ , it can be expanded in the wavenumber domain:

$$\begin{aligned} (\hat{\rho} \tilde{J}) &= \begin{bmatrix} \rho_{xx} & \rho_{xy} & \rho_{xz} \\ \rho_{yx} & \rho_{yy} & \rho_{yz} \\ \rho_{zx} & \rho_{zy} & \rho_{zz} \end{bmatrix} \begin{bmatrix} iv\tilde{T}_J + iu\tilde{P}'_J \\ -iu\tilde{T}_J + iv\tilde{P}'_J \\ k^2\tilde{P}_J \end{bmatrix} \\ &= \begin{bmatrix} \rho_{xx}(iv\tilde{T}_J + iu\tilde{P}'_J) + \rho_{xy}(-iu\tilde{T}_J + iv\tilde{P}'_J) + \rho_{xz}k^2\tilde{P}_J \\ \rho_{yx}(iv\tilde{T}_J + iu\tilde{P}'_J) + \rho_{yy}(-iu\tilde{T}_J + iv\tilde{P}'_J) + \rho_{yz}(k^2\tilde{P}_J) \\ \rho_{zx}(iv\tilde{T}_J + iu\tilde{P}'_J) + \rho_{zy}(-iu\tilde{T}_J + iv\tilde{P}'_J) + \rho_{zz}(k^2\tilde{P}_J) \end{bmatrix} \end{aligned} \quad (30)$$

According to Equation 28, the component in z direction can be deduced.

$$\hat{z} \cdot (\nabla \times (\hat{\rho}J)) = \begin{bmatrix} i & j & k \\ \frac{\partial}{\partial x} & \frac{\partial}{\partial y} & \frac{\partial}{\partial z} \\ (\rho J)_x & (\rho J)_y & (\rho J)_z \end{bmatrix} = \frac{\partial}{\partial x}(\rho J)_y - \frac{\partial}{\partial y}(\rho J)_x = 0 \quad (31)$$

Here,

$$\begin{aligned} (\rho J)_x &= \rho_{xx}(iv\tilde{T}_J + iu\tilde{P}'_J) + \rho_{xy}(-iu\tilde{T}_J + iv\tilde{P}'_J) + \rho_{xz}k^2\tilde{P}_J, \\ (\rho J)_y &= \rho_{yx}(iv\tilde{T}_J + iu\tilde{P}'_J) + \rho_{yy}(-iu\tilde{T}_J + iv\tilde{P}'_J) + \rho_{yz}(k^2\tilde{P}_J), \\ (\rho J)_z &= \rho_{zx}(iv\tilde{T}_J + iu\tilde{P}'_J) + \rho_{zy}(-iu\tilde{T}_J + iv\tilde{P}'_J) + \rho_{zz}(k^2\tilde{P}_J). \end{aligned}$$

Now Equation 31 can be expanded as follows:

$$(\rho_{xx}v^2 + \rho_{yy}u^2 - 2\rho_{xy}uv)\tilde{T}_J + (uv(\rho_{xx} - \rho_{yy}) + (v^2 - u^2)\rho_{xy})\tilde{P}'_J + ik^2(u\rho_{yz} - v\rho_{xz})\tilde{P}_J = 0 \quad (32)$$

In order to easily express Equation 32, we set three coefficients, as follows:

$$\begin{aligned} a &= v^2\rho_{xx} - 2uv\rho_{xy} + u^2\rho_{yy}, \\ b &= uv(\rho_{xx} - \rho_{yy}) + (v^2 - u^2)\rho_{xy}, \\ c &= i(v\rho_{xz} - u\rho_{yz}). \end{aligned}$$

Hence Equation 32 can be rewritten as:

$$a\tilde{T}_J + b\tilde{P}'_J - ck^2\tilde{P}_J = 0 \quad (33)$$

Based on Equation 33, we can obtain the following:

$$\tilde{T}_J = \frac{ck^2\tilde{P}_J - b\tilde{P}'_J}{a} \quad (34)$$

$$\tilde{T}'_J = \frac{ck^2\tilde{P}'_J - b\tilde{P}''_J}{a} \quad (35)$$

According to Equation 29, the component in z direction can be deduced.

$$\hat{z} \cdot \nabla \times \nabla \times (\hat{\rho}J) = 0 \quad (36)$$

Equation 36 can be expanded as follows:

$$\begin{aligned} \hat{z} \cdot \nabla \times \nabla \times (\hat{\rho}J) &= \tilde{P}''_J(v^2\rho_{yy} - u^2\rho_{xx}) + \tilde{T}'_J[k^2\rho_{yy} - uv(\rho_{yy} + \rho_{xx})] \\ &\quad + i2k^2u\rho_{xz}\tilde{P}'_J + ik^2(v\rho_{xz} - u\rho_{yz})\tilde{T}_J + ik^2(u - v)\rho_{zz}\tilde{P}_J \\ &= 0 \end{aligned} \quad (37)$$

Combing Equations 34, 35, 36 and 37 the following is obtained:

$$\begin{aligned} \tilde{P}''_J(v^2\rho_{yy} - u^2\rho_{xx}) + \frac{ck^2\tilde{P}'_J - b\tilde{P}''_J}{a}[k^2\rho_{yy} - uv(\rho_{yy} + \rho_{xx})] \\ + i2k^2u\rho_{xz}\tilde{P}'_J + ik^2(v\rho_{xz} - u\rho_{yz})\frac{ck^2\tilde{P}_J - b\tilde{P}'_J}{a} \\ + ik^2(u - v)\rho_{zz}\tilde{P}_J = 0 \end{aligned} \quad (38)$$

Here,

$$\begin{aligned} a &= v^2\rho_{xx} - 2uv\rho_{xy} + u^2\rho_{yy}, \\ b &= uv(\rho_{xx} - \rho_{yy}) + (v^2 - u^2)\rho_{xy}, \\ c &= i(v\rho_{xz} - u\rho_{yz}), \end{aligned}$$

Equation 38 can be simplified using Equation 39:

$$d\tilde{P}''_J + 2e\tilde{P}'_J - (c^2 + af)\tilde{P}_J = 0 \quad (39)$$

Here,

$$\begin{aligned} d &= (v^2 - u^2)(\rho_{xx}\rho_{yy} - \rho_{xy}^2) \\ e &= u^2[iv(\rho_{xz}\rho_{xy} - \rho_{yz}\rho_{xx}) + iu(\rho_{yz}\rho_{xy} - \rho_{xz}\rho_{yy})], \\ f &= i(u - v)\rho_{zz}. \end{aligned}$$

Based on Equations 34 and 39, the basic solution of the electromagnetic field can be calculated.

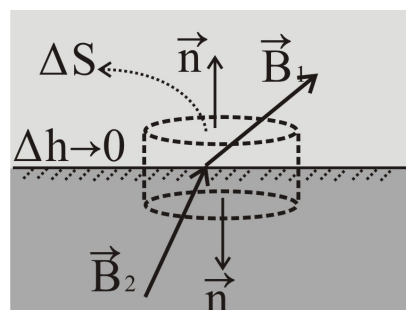


FIGURE 2. The boundary condition of magnetic field.

### B. BOUNDARY CONDITION OF INTERNAL LAYER

For the magnetic induction intensity  $\mathbf{B}$  at the boundary between the two layers, we can analyse its condition using the model shown in Figure 2. A small volume is employed to study the boundary condition of  $\mathbf{B}$ . According to the Gauss's theorem the following equation is obtained:

$$\oint_S \tilde{\mathbf{B}} \cdot d\tilde{\mathbf{S}} = 0 \quad (40)$$

When the height of the volume is small enough, Equation 40 can be rearranged as:

$$\tilde{\mathbf{B}}_1 \cdot d\tilde{\mathbf{S}}_1 + \tilde{\mathbf{B}}_2 \cdot d\tilde{\mathbf{S}}_2 = 0 \quad (41)$$

Based on Equation 41, the relationship of  $\tilde{\mathbf{B}}_1$  and  $\tilde{\mathbf{B}}_2$  can be obtained.

$$\tilde{\mathbf{B}}_1 = \tilde{\mathbf{B}}_2 \quad (42)$$

Here, the magnetic permittivity  $\mu_1 = \mu_2 = \mu_0$ .

Furthermore, Equation 42 can be rewritten as:

$$H_1 = H_2 \quad (43)$$

Based on the above

$$\tilde{P}'_H = 0 \quad (44)$$

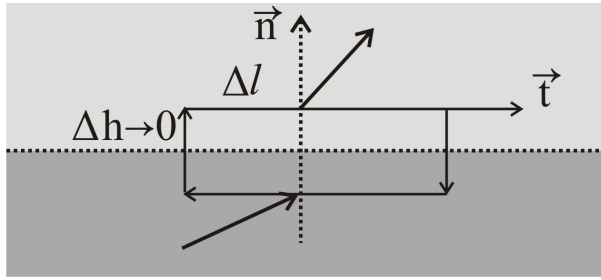


FIGURE 3. The boundary condition of the electrical field.

For the electrical field  $E$  at the boundary between the two layers, the condition can be analyzed using the model as shown in Figure 3. A small rectangle can be employed to study the boundary. For the constant electrical field, the integrated electric field along any closed path is zero, as shown below:

$$\oint_l \vec{E} \cdot d\vec{l} = 0 \quad (45)$$

When the height  $h \rightarrow 0$ , Equation 45 can be expanded as follows:

$$\oint_l \vec{E} \cdot d\vec{l} = \vec{E}_1 \cdot \vec{t} \Delta l - \vec{E}_2 \cdot \vec{t} \Delta l = 0 \quad (46)$$

Hence, we can obtain the continuous tangential component of  $E$ .

Based on Equations 44, 45 and 46, the boundary condition implies as in (Yin, 1999):

$$[\tilde{P}_H] = 0, [\tilde{P}'_H] = 0, [\tilde{P}_J] = 0 \text{ and } [(d\tilde{P}'_J + e\tilde{P}_J)/a] = 0 \quad (47)$$

Here,  $[ ]$  indicates jump condition.

### C. BOUNDARY CONDITION AT THE GROUND SURFACE

At the ground surface, there are two point current sources;  $r_A$  and  $r_B$  indicate the positions of positive pole and negative pole.

$$+I : r_A = (x_A, y_A, 0), \quad -I : r_B = (x_B, y_B, 0) \quad (48)$$

For the two point sources, the relationship between the current density and current intensity can be described as:

$$\nabla \cdot J = I\{\delta(r_A - r) - \delta(r_B - r)\}\delta(z) \quad (49)$$

Here,  $r$  is the distance between the point source and considered point at the ground surface.

The integration from over ground surface to the ground surface  $z = 0$ ,  $J_z(z = 0^-) = 0$ . Thus the integration of Equation 49 can be expressed as follows:

$$J_z(z = 0^+) = I\{\delta(r_A - r) - \delta(r_B - r)\} \quad (50)$$

The two domains Fourier transformation of Equation 50 is

$$\tilde{J}_z(k, 0^+) = I(e^{-ikr_A} - e^{-ikr_B}) \quad (51)$$

From Equation 14, the relationship between  $\tilde{J}_Z$  and  $\tilde{P}_J$  is as follows:

$$\tilde{J}_Z = k^2 \tilde{P}_J \quad (52)$$

Here,  $k = u_x + v_y, k^2 = \mu^2 + v^2$

Hence,  $\tilde{P}_J$  can be expressed as:

$$\tilde{P}_J(k, 0^+) = \frac{I}{k^2}(e^{-ikr_A} - e^{-ikr_B}) \quad (53)$$

Equation 53 is obtained by combining Equations 14 and 47.

$$D_J = [\tilde{P}_J]_{-}^{+} = \tilde{P}_J(J, 0^+) = \frac{I}{k^2}\{e^{-ikr_A} - e^{-ikr_B}\} \quad (54)$$

Here,  $D_J$  is the jump across at the boundary of  $z = 0$ .

Furthermore, according to Equation 12, the horizontal projection of the magnetic field can be given as below:

$$\tilde{H}_h = \tilde{H}_{x,x} + \tilde{H}_{y,y} \quad (55)$$

This can further be expanded to:

$$\begin{aligned} \tilde{H}_h &= \tilde{H}_x \hat{x} + \tilde{H}_y \hat{y} \\ &= [i(v\tilde{T}_H + u\tilde{P}'_H)] \hat{x} + [i(-u\tilde{T}_H + v\tilde{P}'_H)] \hat{y} \\ &= i(v\hat{x} - u\hat{y}) \hat{T}_H + i(u\hat{x} + v\hat{y}) \hat{P}'_H \end{aligned} \quad (56)$$

Because,  $\hat{k} \times \hat{z} = \begin{vmatrix} \hat{x} & \hat{y} & \hat{z} \\ u & v & 0 \\ 0 & 0 & 1 \end{vmatrix} = v\hat{x} - u\hat{y}$  and  $\hat{z}(\nabla \times H) = \hat{z}(J), T_H = P_J$  (as shown in Equation 19).

Hence Equation 19 can be rewritten

$$\begin{aligned} \tilde{H}_h &= i(v\hat{x} - u\hat{y}) \hat{T}_H + i(u\hat{x} + v\hat{y}) \hat{P}'_H \\ &= i(\hat{k} \times \hat{z}) \tilde{P}_J + i\hat{k} \cdot \tilde{P}'_H \end{aligned} \quad (57)$$

Here,  $k = u\hat{x} + v\hat{y}, k^2 = \mu^2 + v^2$

The expression of  $\tilde{H}_h$  can be rewritten using Equation 58:

$$\tilde{H}_h = i(k \times z) \tilde{P}_J + ik \tilde{P}'_H \quad (58)$$

Equation 58 can be adapted by multiplying  $ik$ :

$$\begin{aligned} ik \cdot \tilde{H}_h &= ik \cdot (i(k \times z) \tilde{P}_J + ik \tilde{P}'_H) \\ &= i(u\hat{x} + v\hat{y}) \cdot (u\hat{x} - v\hat{y}) \tilde{P}_J - k^2 \tilde{P}'_H \end{aligned} \quad (59)$$

Because  $(u\hat{x} + v\hat{y}) \cdot (u\hat{x} - v\hat{y}) \tilde{P}_J = 0$ , the following is obtained:

$$P'_H = -ik \cdot \tilde{H}_h / k^2 \quad (60)$$

Hence, the jump across can be written as:

$$[P'_H]_{-}^{+} = -ik \cdot [\tilde{H}_h]_{-}^{+} / k^2 \quad (61)$$

According to Biot-Savart's law, the horizontal components of the magnetic field are Yin [11].

$$H_h(r) = \frac{I(d \times z)z}{4\pi} \int_{r_B}^{r_A} \frac{ds_0}{|r - r_0|^3} \quad (62)$$

Here,  $d = \frac{(r_A - r_B)}{|r_A - r_B|}$ ,  $r = (x, y, z)$ ,  $r_0 = (x_0, y_0, z_0)$ ,  $ds_0$  is the length of the line element.

Equation 62 can be transformed into the wavenumber domain.

$$\tilde{H}_h(k, z) = \frac{I}{2}(\hat{d} \times \hat{z})\text{sign}(z) \int_{r_B}^{r_A} e^{-ik \cdot r_0 - k|z|} ds_0 \quad (63)$$

Thus, the integration from  $z^-$  to  $z^+$ :

$$\begin{aligned} \left| \tilde{H}_h(k, z) \right|_{-}^{+} &= I(\hat{d} \times \hat{z}) \int_{r_B}^{r_A} e^{-ik \cdot r_0} ds_0 \\ &= I(\hat{d} \times \hat{z}) \frac{e^{-ik \cdot r_A} - e^{-ik \cdot r_B}}{-ik \cdot \hat{d}} \end{aligned} \quad (64)$$

The jump cross can be described using the following:

$$D_H = [P'_H]_{-}^{+} = I \frac{k \cdot (\hat{d} \times \hat{z})}{k^2(k \cdot \hat{d})} \{e^{-ik \cdot r_A} - e^{-ik \cdot r_B}\} \quad (65)$$

### III. COMPUTATION OF $\tilde{P}_J(k, z)$ AND $\tilde{P}_H(k, z)$

#### A. COMPUTATION OF $\tilde{P}_J(k, z)$

Based on the conditions of the inner layer,  $\tilde{P}_J(k, z)$  is computed by solving Equation 33 using the layered model of uniform electric anisotropy.

$$\tilde{P}_J(z) = A \exp(-\alpha_l z) \quad (66)$$

Here,  $A$  is arbitrary constant.

Inserting Equation 66 into Equation 33:

$$d\alpha_l^2 - 2e\alpha_l - (c^2 + \alpha_l f_l) = 0 \quad (67)$$

$\alpha_l$  can be computed, as follows:

$$\alpha_l^{\pm} = \beta_l \pm \gamma_l \quad (68)$$

Here,

$$\begin{aligned} \beta_l &= \frac{e_l}{d_l}, \\ \gamma_l &= \frac{\sqrt{4e_l^2 + 4d_l(c_l^2 + d_l f_l)}}{2d_l} = \frac{1}{d_l} \sqrt{\alpha_l \det \bar{\rho}_l} \end{aligned}$$

and

$$\bar{\rho}_l = \begin{bmatrix} \rho_{xx} & \rho_{xy} & \rho_{xz} \\ \rho_{yx} & \rho_{yy} & \rho_{yz} \\ \rho_{zx} & \rho_{zy} & \rho_{zz} \end{bmatrix}.$$

The completed solution of  $\tilde{P}_J$  in the layer  $l$  is:

$$\tilde{P}_J(z) = A_l^+ e^{-\alpha_l^+(z-z_l)} + A_l^- e^{-\alpha_l^-(z-z_l)} \quad (69)$$

Here,  $A_l^+$  is the amplitude of the up going wave and  $A_l^-$  is the amplitude of the down going wave.  $\alpha_l^+$  and  $\alpha_l^-$  are wave number of up going wave and down going wave.

Therefore, at the boundary of  $l$ th layer and  $(l + 1)$ th layer, the following is obtained:

$$\tilde{P}_J(z = z_{l+1}^-) = A_l^+ e^{-\alpha_l^+ h_l} + A_l^- e^{-\alpha_l^- h_l} \quad (70)$$

$$\tilde{P}_J(z = z_{l+1}^+) = A_{l+1}^+ + A_{l+1}^- \quad (71)$$

According to the boundary condition of  $[\tilde{P}_J] = 0$ :

$$\tilde{P}_J(z = z_{l+1}^-) = \tilde{P}_J(z = z_{l+1}^+)$$

or

$$A_l^+ e^{-\alpha_l^+ h_l} + A_l^- e^{-\alpha_l^- h_l} = A_{l+1}^+ + A_{l+1}^- \quad (72)$$

According to the boundary condition of  $[(d\tilde{P}_J + e\tilde{P}_J)/a] = 0$ :

$$\begin{aligned} [d_l \tilde{P}'_J(z_l^+) + e_l \tilde{P}'_J(z_l^-)] / \alpha_l \\ = [d_{l+1} \tilde{P}'_J(z_{l+1}^+) + e_{l+1} \tilde{P}'_J(z_{l+1}^-)] / \alpha_{l+1} \end{aligned} \quad (73)$$

Inserting Equation 71 and 72 into Equation 73:

$$\xi_l (A_l^+ e^{-\alpha_l^+ h_l} - A_l^- e^{-\alpha_l^- h_l}) = \xi_{l+1} (A_{l+1}^+ - A_{l+1}^-) \quad (74)$$

Here,  $\xi_l = \sqrt{\det \rho_l / \alpha_l}$

Let  $B_l = \xi_l \frac{A_l^+ - A_l^-}{A_l^+ + A_l^-}$  and  $B_{l+1} = \xi_{l+1} \frac{A_{l+1}^+ - A_{l+1}^-}{A_{l+1}^+ + A_{l+1}^-}$

Equation 74 can thus be rewritten as:

$$\begin{aligned} \xi_l (A_l^+ e^{-\alpha_l^+ h_l} - A_l^- e^{-\alpha_l^- h_l}) \\ = \xi_{l+1} (A_{l+1}^+ - A_{l+1}^-) \\ = B_{l+1} (A_{l+1}^+ + A_{l+1}^-) \end{aligned} \quad (75)$$

Equation 72 can be rewritten as:

$$\xi_l (A_l^+ e^{-\alpha_l^+ h_l} + A_l^- e^{-\alpha_l^- h_l}) = \xi_{l+1} (A_{l+1}^+ + A_{l+1}^-) \quad (76)$$

Combing Equations 75 and 76

$$\begin{cases} \xi_l (A_l^+ e^{-\alpha_l^+ h_l} + A_l^- e^{-\alpha_l^- h_l}) = \xi_{l+1} (A_{l+1}^+ + A_{l+1}^-) \\ \xi_l (A_l^+ e^{-\alpha_l^+ h_l} - A_l^- e^{-\alpha_l^- h_l}) = B_{l+1} (A_{l+1}^+ + A_{l+1}^-) \end{cases} \quad (77)$$

From Equation 77,  $A_l^+$  and  $A_l^-$  can be computed.

$$A_l^+ = \frac{(\xi_l + B_{l+1})(A_{l+1}^+ + A_{l+1}^-) e^{\alpha_l^+ h_l}}{2\xi_l} \quad (78)$$

$$A_l^- = \frac{(\xi_l - B_{l+1})(A_{l+1}^+ + A_{l+1}^-) e^{\alpha_l^- h_l}}{2\xi_l} \quad (79)$$

$A_l^+$  and  $A_l^-$  are inserted as follows:

$$B_l = \xi_l \frac{B_{l+1} + \xi_l \frac{e^{\alpha_l^+ h_l} - e^{\alpha_l^- h_l}}{e^{\alpha_l^+ h_l} + e^{\alpha_l^- h_l}}}{\xi_l + B_{l+1} \frac{e^{\alpha_l^+ h_l} - e^{\alpha_l^- h_l}}{e^{\alpha_l^+ h_l} + e^{\alpha_l^- h_l}}} \quad (80)$$

Solution  $\alpha_l^{\pm} = \beta_l \pm \gamma_l$  is substituted into  $\frac{e^{\alpha_l^+ h_l} - e^{\alpha_l^- h_l}}{e^{\alpha_l^+ h_l} + e^{\alpha_l^- h_l}}$ .

$$\tanh(\gamma_l h_l) = \frac{e^{\gamma_l h_l} - e^{-\gamma_l h_l}}{e^{\gamma_l h_l} + e^{-\gamma_l h_l}} \quad (81)$$

Therefore

$$B_l = \xi_l \frac{B_{l+1} + \xi_l \tanh(\gamma_l h_l)}{\xi_l + B_{l+1} \tanh(\gamma_l h_l)} \quad (82)$$

For the last layer there is no down going wave thus  $A_1^- = 0.0$ . Hence, we can obtain  $B_1$  for the last layer as shown below:

$$B_1 = \xi_1 \tag{83}$$

For the surface, the  $A_1^+$  and  $A_1^-$  can be calculated by  $D_J = A_1^+ + A_1^-$  and  $B_1 = \xi_1 \frac{A_1^+ - A_1^-}{A_1^+ + A_1^-}$ .

$$A_1^+ = \frac{\xi_1 + B_1}{2\xi_1} D_J \tag{84}$$

$$A_1^- = \frac{\xi_1 - B_1}{2\xi_1} D_J \tag{85}$$

And  $\tilde{P}'_J(0^+)$  can be calculated.

$$\tilde{P}'_J(0^+) = -(\beta_1 + \gamma_1 B_1 / \xi_1) D_J \tag{86}$$

**B. COMPUTATION OF  $\tilde{P}_H(k, z)$**

For the purpose of obtaining the magnetic field,  $\tilde{P}_H(k, z)$  is calculated. According to Equations 27 and 46,  $\tilde{P}_H(k, z)$  can be expressed using integration.

$$\tilde{P}_H(z = z_0) = \frac{1.0}{2k} \int_0^{+\infty} \tilde{T}_J(z) e^{-k|z-z_0|} dz - D_H e^{-k|z_0|} \tag{87}$$

For the ground surface:  $z = 0.0$

$$\tilde{P}_H(0) = \frac{1.0}{2k} \int_0^{+\infty} \tilde{T}_J(z) e^{-kz} dz - D_H \tag{88}$$

$$\tilde{P}_H(0) = \frac{1.0}{2k} \int_0^{+\infty} \tilde{T}_J(z) e^{-kz} dz + D_H \tag{89}$$

**IV. COMPUTATION OF APPARENT RESISTIVITY**

Based on above work, the relationship between the current density, magnetic field and the electric field can be expressed by the equation.

$$[\tilde{J}_x(0^+) \quad \tilde{J}_y(0^+) \quad \tilde{J}_z(0^+)]^T = \begin{bmatrix} i\{vc_1 k^2 \tilde{P}_J(0^+) + (u\alpha_1 - vb_1) \tilde{P}'_J\} / \alpha_1 \\ i\{-\mu c_1 k^2 \tilde{P}_J(0^+) + (u\alpha_1 + vb_1) \tilde{P}'_J\} / \alpha_1 \\ k^2 \tilde{P}'_J(0^+) \end{bmatrix} \tag{90}$$

$$\begin{bmatrix} \tilde{H}_x(0^+) \\ \tilde{H}_x(0^-) \\ \tilde{H}_y(0^+) \\ \tilde{H}_y(0^-) \\ \tilde{H}_z(0) \end{bmatrix} = \begin{bmatrix} i\{v\tilde{P}_J(0^+) + u\tilde{P}'_H(0^+)\} \\ iuk\tilde{P}_H(0^+) \\ i\{-u\tilde{P}_J(0^+) + v\tilde{P}'_H(0^+)\} \\ ivk\tilde{P}_H(0^+) \\ k^2\tilde{P}_H(0^+) \end{bmatrix} \tag{91}$$

$$\begin{bmatrix} \tilde{E}_x(0^+) \\ \tilde{E}_y(0^+) \\ \tilde{E}_z(0^+) \end{bmatrix} = \begin{bmatrix} \rho_{xx} & \rho_{xy} & \rho_{xz} \\ \rho_{yx} & \rho_{yy} & \rho_{yz} \\ \rho_{zx} & \rho_{zy} & \rho_{zz} \end{bmatrix} \begin{bmatrix} \tilde{J}_x(0^+) \\ \tilde{J}_y(0^+) \\ \tilde{J}_z(0^+) \end{bmatrix}$$

The field in the space domain can be calculated by Fourier transform as:

$$F(x, y) = \frac{1}{2\pi} \int_{-\infty}^{+\infty} \int_{-\infty}^{+\infty} \tilde{F}(\mu, \nu) \exp[i(\mu x + \nu y)] d\mu d\nu \tag{92}$$

Finally, the apparent resistivity can be calculated as: (93)

$$\rho_a(r) = G \frac{Er(0^+)}{I} \tag{93}$$

Here,  $G$  is the coefficient of measurement system.

**V. NUMERICAL SIMULATION**

For modeling, the Schlumberger array is employed to simulate the geological model of the goaf [18]. The geological model is shown in Figure 4(a) and the schematic diagram of the measurement is shown in Figure 4(b). Through the whole measurement process, 24 values of apparent resistivity around the origin of the coordinate are calculated. These values are used to form the ellipse. Finally, the shape of ellipse assists in the analysis of the information of the fractures in the fractured zone. Different models with different stratigraphic dips and strikes are used to study the relation between apparent resistivity and the geological occurrence of fractured zone. In addition, all the simulations have been done by FORTRAN code made by author.

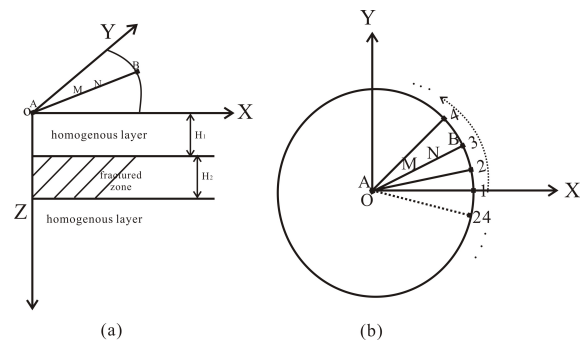


**FIGURE 4.** (a) is the geological model of the goaf and Schlumberger array being used to do the modeling shown as an electrodes array AMNB. Fig. 4(b) shows the electrode array at the ground surface where 24 values of the apparent resistivity around the origin of the coordinate are calculated.

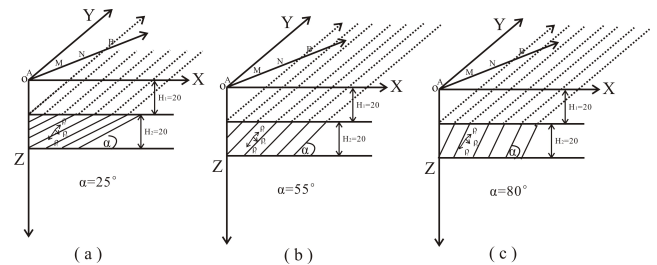


**FIGURE 5.** Three geological models of the goaf with different stratigraphic dips which are 25, 55 and 80 degrees respectively. The stratigraphic strikes are parallel with the Y axis. The resistivity of the upper and lower homogeneous layers is 100 ohm-m and for the fractured zone,  $\rho_T$  and  $\rho_N$  are 25 ohm-m and 100 ohm-m respectively.

**A. NUMERICAL SIMULATION 1**

The purpose of the numerical simulation is to investigate the stratigraphic dips of the fractures in the fractured zone in the goaf. As shown in Figure 5, the fractured zone is sandwiched by the upper and lower homogeneous layers.

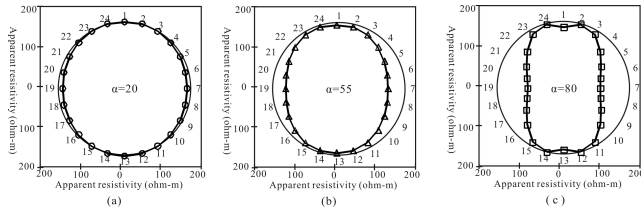


**FIGURE 6.** The numerical modeling results of the goaf. The distribution of the apparent resistivity, as shown (a), (b) and (c) correspond to the geological models in Figure 5 (a), (b) and (c).

There are three goaf models where stratigraphic dips of fractures in the fractured zone are  $25^\circ$ ,  $55^\circ$  and  $80^\circ$  respectively and the stratigraphic strikes are parallel with Y-axis. For the fractured zone, the longitudinal resistivity  $\rho_T$  and the transverse resistivity  $\rho_N$  are 25 ohm-m and 100 ohm-m respectively. The resistivity of the upper and lower homogenous layers is 100 ohm-m. The length of AB is set to be 60 m. According to the principle of the electrical method, it can detect the geological information of the fractured zone in the goaf. The modeling results of the geological models as shown in Figure 5 are described in Figure 6. In Figure 6, the distribution of the apparent resistivity, as shown (a), (b) and (c) correspond to the geological models (a), (b) and (c), described in Figure 5. As described in Figure 6, the shapes of the distribution of the apparent resistivity are different from each other. This difference is used to analyze the geological information of the fractured zone of the goaf.

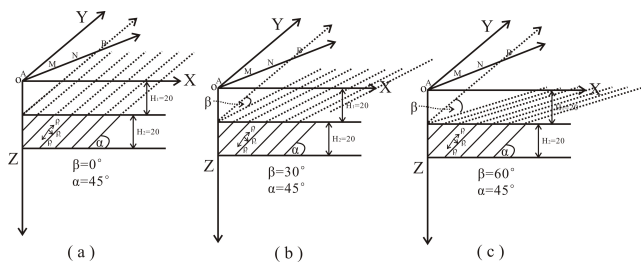


**FIGURE 7.** Three geological models of the goaf with different stratigraphic dips which are 00, 300 and 600 respectively. The stratigraphic strikes are parallel with the Y axis. Moreover, the resistivity of the upper and lower homogenous layers is 100 ohm-m and the fractured zone  $\rho_T$  and  $\rho_N$  are 25 ohm-m and 100 ohm-m respectively.

### B. NUMERICAL SIMULATION 2

The purpose of the numerical simulation is to investigate the electrical response due to existence of the stratigraphic strikes. As shown in Figure 7, the stratigraphic strike angles are 00, 300 and 600 respectively. The stratigraphic dips of the geological models are all  $45^\circ$ . The resistivity of the upper and lower homogenous layers is 100 ohm-m and for the fractured zone  $\rho_T$  and  $\rho_N$  are 25 ohm-m and 100 ohm-m respectively. The modeling methods are the same as the numerical simulation. The modeling results of geological models in Figure 7 are shown in Figure 8. In Figure 8, the distribution of the apparent resistivity, as shown

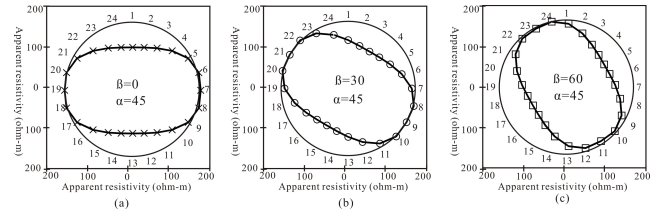


**FIGURE 8.** Numerical modeling results of the goaf. The distribution of the apparent resistivity, as shown in (a), (b) and (c), correspond to the geological models in Figure 7 (a), (b) and (c).

in (a), (b) and (c) correspond to the geological models in Figure 7 (a), (b) and (c). As described in Figure 8, the shapes of the distribution of apparent resistivity are different from each other due to the difference of the stratigraphic strikes. Hence, the difference of the shapes of the distribution of the apparent resistivity can assist in the analysis of the geological information of the fractured zone of the goaf.

### VI. CONCLUSIONS

In this paper, the following conclusions are obtained from the theoretical research and numerical simulation:

- 1) Electrical anisotropy of formation caused by the stratigraphic dip and strike direction exhibit obvious characteristics in the polar coordinates. The information of the water conducted fractured zone can be analyzed in detail through these characteristics.
- 2) The modeling results show that the distribution of apparent resistivity for the formation of water conducted fractures exhibit an ellipse shape in the polar coordinate system through the specially designed measurement system. The shape of the ellipse is decided by the stratigraphic dip and direction of the long axis of ellipse.
- 3) Based on above results, the earth information of water conducted fracture can be estimated by the DC resistivity method with the specially designed measurement system. The application of the method will enhance the ability of exploring the goaf in coal fields so as to improve safety during coal mining.

### ACKNOWLEDGEMENT

The authors would like to thank three anonymous reviewers for critical reviews and comments.

### REFERENCES

- [1] T. M. Liu and H. L. Qin, "Economic analysis of safety accidents in China coal mining," *Coal Mine Safety*, vol. 377, no. 1, pp. 70–72, 2006.
- [2] N. G. Dong, L. Y. Pan, and J. B. Li, "Talk about of control measures of major hazard sources," *Shandong Coal Sci. Technol.*, vol. 1, no. 1, pp. 200–201, 2011.
- [3] C. A. Balanis, P. W. Shepard, F. T. C. Ting, and W. F. Kardosh, "Anisotropic electrical properties of coal," *IEEE Trans. Geosci. Remote Sens.*, vol. 18, no. 3, pp. 250–256, Jul. 1980.
- [4] W. F. Brace and A. F. Orange, "Electrical resistivity changes in saturated rocks during fracture and frictional sliding," *J. Geophys. Res.*, vol. 73, no. 4, pp. 1433–1445, 1968.



- [5] M. W. Asten, "The influence of electrical anisotropy on Mise À La Masse surveys," *Geophys. Prospecting*, vol. 22, no. 2, pp. 238–245, 1974.
- [6] M. J. S. Matias and G. M. Habberjam, "The effect of structure and anisotropy on resistivity measurements," *Geophysics*, vol. 51, no. 4, pp. 964–971, 1986.
- [7] M. Chlamtac and F. Abramovici, "The electromagnetic fields of a horizontal dipole over a vertically inhomogeneous and anisotropic earth," *Geophysics*, vol. 46, no. 6, pp. 904–915, 1981.
- [8] B. I. Anderson, T. Barber, and S. C. Gianzero, "The effect of crossbedding anisotropy on induction tool response," in *Proc. Trans. 39th SPWLA*, 1998, pp. 137–149.
- [9] D. C. Li, B. T. Ge, and J. W. Hu, "Predicted mechanism and experiment of resistivity method for the coal mine," *Coal Geology Exploration*, vol. 27, no. 6, pp. 62–64, 1999.
- [10] S. L. Lv and J. S. He, "Electrical property measurements for the outburst coal mass," *J. Center South Univ. Technol.*, vol. 6, no. 4, pp. 511–514, 1998.
- [11] C. Yin and P. Weidelt, "Goelectrical fields in a layered earth with arbitrary anisotropy," *Geophysics*, vol. 64, no. 2, pp. 426–434, 1999.
- [12] J.-S. Shen, N.-C. Guo, and B.-Y. Su, "Response characteristics of apparent resistivity of anisotropic laminar formation in direct current electric sounding," *J. China Univ. Petroleum*, vol. 33, no. 3, pp. 59–65, 2009.
- [13] C.-Y. Han, J.-J. Chen, X.-H. Xia, and J.-H. Wang, "Three-dimensional stability analysis of anisotropic and non-homogeneous slopes using limit analysis," *J. Central South Univ.*, vol. 21, no. 3, pp. 1142–1147, 2014.
- [14] Y. Jiang, H. Zhu, and Z. Li, "A new compound faults detection method for rolling bearings based on empirical wavelet transform and chaotic oscillator," *Chaos, Solitons, Fractals*, vol. 89, pp. 8–19, Aug. 2016.
- [15] W. Sui *et al.*, "Interactions of overburden failure zones due to multiple-seam mining using longwall caving," *Bull. Eng. Geol. Environ.*, vol. 74, no. 3, pp. 1019–1035, 2015.
- [16] M. N. Nabighian, *Electromagnetic Methods in Applied Geophysics*. Tulsa, OK, USA: Soc Exploration Geophysics, 1991, pp. 47–99.
- [17] G. Backus, "A class of self-sustaining dissipative spherical dynamos," *Ann. Phys.*, vol. 4, no. 4, pp. 372–447, 1958.
- [18] V. Henriques and R. Malekian, "Mine safety system using wireless sensor network," *IEEE Access*, vol. 4, pp. 3511–3521, Jun. 2016.



**REZA MALEKIAN** (M'12) is currently a Senior Lecturer with the Department of Electrical, Electronic, and Computer Engineering, University of Pretoria, Pretoria, South Africa, and an Assistant Professor (attache) with the Department de Ingeniería Informática, Universidad de Santiago de Chile, Chile. His current research interests include advanced sensor networks, Internet of Things, and mobile communications. He is also a Chartered Engineer and a Professional Member of the British Computer Society. He is an associate editor for the IEEE INTERNET OF THINGS JOURNAL.



**JINGCUN YU** received the Ph.D. degree from the Department of Applied Geophysics, China University of Mining and Technology, China, in 2000. He is currently with the China University of Mining and Technology, China, as a Professor. His research interest is mine geophysics.



**XIHUI FENG** received the bachelor's degree from the China University of Mining and Technology, in 1989. He was promoted to Senior Engineer at Professor Grade, in 2008. He is currently the Deputy Director of the Key Laboratory of Coal Resource Exploration and Comprehensive Utilization with the Ministry of Land and Resources.



**BENYU SU** received the Ph.D. degree from the Faculty of Earth Resource of Engineering Department, Kyushu University, Japan, in 2012. He is currently an Assistant Professor with the China University of Mining and Technology, China. His current research interests are mine and environment geophysics.



**ZHIXIN LIU** received the Ph.D. degree from the Department of Applied Geophysics, China University of Mining and Technology, China, in 2007. He is currently with the China University of Mining and Technology, China, as an Associate Professor. His research interest is mine geophysics.

• • •